RSC Advances

PAPER

View Article Online
View Journal | View Issue

Cite this: *RSC Adv.*, 2024, **14**, 22266

Engineering a sustainable cadmium sulfide/polyethyleneimine-functionalized biochar/chitosan composite for effective chromium adsorption: optimization, co-interfering anions, and mechanisms†

Abdelazeem S. Eltaweil, [ab] Nouf Al Harby, *[c] Mervette El Batouti [b] and Eman M. Abd El-Monaem[b]

A novel eco-friendly adsorbent was fabricated by mixing mushroom-derived cadmium sulfide and polyethyleneimine-functionalized biochar that was fabricated from coffee waste with a chitosan biopolymer. The green-synthesized CdS/PEI-BC/CTS composite was analyzed using several characterization methods to identify its morphological, compositional, and structural characteristics. In addition, the adsorption property of the composite was investigated for hexavalent chromium as a model for anionic heavy metals. The best adsorption conditions to efficiently adsorb Cr(VI) onto CdS/PEI-BC/CTS were scrutinized in the batch mode. The experimental results elucidated that the higher adsorption efficacy for Cr(VI) was 97.89% at pH = 3, Cr(VI) concentration = 50 mg L^{-1}, CdS/PEI-BC/CTS dose = 0.01 g, and temperature = 20 °C. The impact of co-interfering anionic species on Cr(VI) adsorption was identified in simulated wastewater. The recycling property of the CdS/PEI-BC/CTS composite was assessed for ten runs to ensure the applicability of the green composite. The adsorption mechanism and interaction types were proposed on the basis of kinetic and isotherm studies, along with analysis tools. The mechanistic study proposed that the Cr(VI) adsorption onto CdS/PEI-BC/CTS occurred *via* chemical and physical pathways, including protonation, electrostatic interactions, reduction, and coordination bonds.

Received 11th May 2024
Accepted 1st July 2024

DOI: 10.1039/d4ra03479a

rsc.li/rsc-advances

1. Introduction

Industrialization revolution is recently prospering in many countries, bringing about an all-important blossom in the economy. Nonetheless, this revolution of varied industries has a series of bottlenecks like environmental pollution. Water pollution is one of the concerning disadvantages of industrialization revolution, in which industrial drainage contains several fatal contaminants, including heavy metals, nitrophenol, dyes, petroleum wastes, and pharmaceutical residuals.

Chromium is one of the most dangerous heavy metals that is categorized among the most harmful sixteen heavy metals.[1,2] Mainly, chromium is involved in essential industries such as leather processing, metal cleaning, pigment synthesis, mining, and electroplating. Generally, chromium could naturally exist in four oxidation states, where trivalent (Cr(III)) and hexavalent (Cr(VI)) are the dominant valence states.[3] Notably, Cr(VI) is assorted in group (1) by the International Agency for Research on Cancer, whereas Cr(III) falls in group (3), which contains non-carcinogenic substances.[4] Consequently, Cr(VI) is more toxic than Cr(III), which is deemed an eco-friendly heavy metal.[5]

Hence, wastewater purification methods, such as adsorption, precipitation, catalysis, membranes, photoreduction and ozonation, have received attention from environmental experts to foster their capability in the removal of this persistent metal from wastewater.[6–11] Strikingly, the nontoxicity, cost-effectiveness, easy processing, recyclability, energy efficiency, and high efficacy of the adsorption technique render it the best choice among other wastewater purification methods.[12,13] Consequently, excessive investigations have been performed to find adsorbents with high capacity and reusability, taking into consideration the capital cost.

Chitosan (CTS) is a linear polyamine biopolymer that involves many amine groups and possesses eminent

[a]*Department of Engineering, College of Engineering and Technology, University of Technology and Applied Sciences, Sultanate of Oman. E-mail: abdelazeemeltaweil@alexu.edu.eg*

[b]*Department of Chemistry, Faculty of Science, Alexandria University, 21934, Alexandria, Egypt. E-mail: emanabdelmonaem5925@yahoo.com; Mervette.elbatouti@.alexu.edu.eg*

[c]*Department of Chemistry, College of Science, Qassim University, Buraidah 51452, Saudi Arabia. E-mail: hrbien@qu.edu.sa*

† Electronic supplementary information (ESI) available. See DOI: https://doi.org/10.1039/d4ra03479a

characteristics such as biocompatibility, hydrophilicity, eco-friendly nature, biodegradability, and high abundance in nature.[14] Chitosan is prepared *via* the simple deacetylation of chitin, which is derived mainly from the external shells of algae, crustaceans, fungi, and insects.[15] The remarkable characteristics of CTS, in addition to its facile fabrication, make it applicable in critical sectors, such as wastewater purification, drug delivery, and catalysis.[16] Various studies have recommended CTS as an excellent adsorbent for many toxic contaminants[17,18] Click or tap here to enter text. Nevertheless, CTS exhibited some limitations, including poor adsorbability and reusability. Pioneering studies have exploited the remarkable features of CTS to develop it, such as the easy functionalization merit, facilitating its bonding with substances that possess high adsorption capacity to boost its efficiency or magnetic substances to foster its recyclability.[19] In addition to this, the easy-molding property of CTS enables its formation in easily separable shapes like membranes, beads, and spheres.[20]

Cadmium sulfide (CdS) is a semiconductor substance that possesses desirable characteristics, such as high chemical stability, easy fabrication approaches, and large surface area, along with its optical and electric properties.[21] Many conventional preparation ways have been applied to fabricate CdS, including precipitation, microwave heating, and hydrothermal. However, these approaches include the utilization of noxious reagents and require high temperatures and specific equipment in some cases.[22] The green method involves the utilization of natural reagents, like plant extract, producing CdS with favorable chemical stability, large surface area, size, and morphology.

Biochar (BC) is a functional carbon substance that is synthesized by pyrolyzing organic feedstocks under a controlled environment.[23] Bountiful feedstocks have been used for preparing BC like poultry manure, forestry residues, algae, crops, agriculture wastes, and sewage sludge. Biochar is well-known for its stinking characteristics, comprising cost-effective, porous structure, high containing oxygen functional groups, excellent mechanical strength, high adsorption capacity, and super-large surface area.[24] Biochar has revealed preeminent adsorption behavior in adsorbing various pollutants with high adsorption efficacy.

In this regard, relevant research studies have been adsorb Cr(VI); for instance, Zhang *et al.* fabricated CTS-stabilized FeS for removing Cr(VI), revealing a maximum adsorption capacity (q_{max}) of 119 mg g^{-1} at pH = 3 using 2.0 g L^{-1} of the adsorbent dose. Furthermore, the adsorption mechanism of Cr(VI) onto CTS-stabilized FeS was supposed to occur by surface complexation, redox reaction, and precipitation.[25] Moreover, the Omer *et al.* study involved preparing Ni–Fe LDH/MWCNT@CA microbeads for removing Cr(VI), fulfilling q_{max} about 384.62 mg g^{-1} at 25 °C and pH = 3. In addition, the microbeads exhibited a slight decrease in the removal% of Cr(VI) in the existence of co-existing anions, such as chloride, sulfate, and nitrate while the cations like potassium, sodium, and calcium almost did not affect the aptitude of Cr(VI) adsorption.[5] In another investigation, Liu *et al.* developed the CTS matrix by the zeolite to adsorb Cr(VI) from wastewater. The q_{max} of Cr(VI) onto the zeolite/CTS composite was 28.47 mg g^{-1} at 30 °C and pH = 3. Analyzing the equilibrium data by kinetic and isotherm models demonstrated that Cr(VI) adsorption fitted the Langmuir adsorption isotherm and pseudo second order kinetics, implying the domination of the chemical interactions in the adsorption process.[26] In this context, Eltaweil and his co-authors developed a new CTS-based adsorbent ($NiFe_2O_4$@-SEH-CTS-SB) to remove the detrimental Cr(VI) from an aqueous medium. The calculated q_{max} of Cr(VI) onto $NiFe_2O_4$@SEH-CTS-SB under the Langmuir isotherm was 373.61 mg g^{-1}. This high adsorption aptitude of $NiFe_2O_4$@SEH-CTS-SB toward adsorbing Cr(VI) is due to the participation of several pathways in the adsorption process, including coulombic interaction, outer-sphere complexation, ion-exchange, surface complexation and coordinate–covalent bonding. Interestingly, the magnetic character of $NiFe_2O_4$@SEH-CTS-SB gives it an easy recycling feature, allowing it to be reused for seven sequential runs with high adsorption efficiency.[27]

Herein, our study is an attempt to fabricate an eco-friendly adsorbent with promising adsorption performance toward the toxic Cr(VI) species. The characteristics of CdS/PEI-BC/CTS were identified using a variety of characterization instruments. The adsorption process of the Cr(VI) ions was optimized in a batch approach. Kinetics and isotherms of the Cr(VI) adsorption onto CdS/PEI-BC/CTS were investigated to determine if the adsorption process is controlled by physical or chemical interactions. In light of the experimental findings and characterization tools, the Cr(VI) adsorption mechanism onto CdS/PEI-BC/CTS was proposed. The cycling test proceeded on CdS/PEI-BC/CTS for ten adsorption runs to inspect its viability and durability.

2. Materials and methods

2.1. Materials

Mushroom plants were obtained from a local market and coffee waste was collected from a café in Alexandria, Egypt. Cadmium chloride monohydrate ($CdCl_2 \cdot H_2O$), polyethyleneimine (PEI), and ethanol (EtOH) were provided by Shanghai Chemical Reagent Co., Ltd. Sodium sulfide nonahydrate ($Na_2S \cdot 9H_2O$) and acetic acid were supplied by Alpha Chemika. Methanol (MeOH) and potassium dichromate ($K_2Cr_2O_7$) were brought from Spectrum Chemical Co. Chitosan (CTS; M.wt. 100 000–300 000 D, DD = 95%) was purchased from Sigma Aldrich.

2.2. Fabrication of cadmium sulfide

Cadmium sulfide was fabricated by a green method as follows: cleaning mushrooms with tap water and double-distilled water, then cutting up into small slices and drying the mushroom slices at 85 °C for 12 h. The crunchy mushroom slices were ground hard by a blender into a fine powder. To prepare the mushroom extract, 10 mg of mushroom powder was suspended in 150 mL of double-distilled water and heated at 85 °C for an hour. After cooling the mushroom extract, it was filtrated by a filter paper. 10 mL of the mushroom extract (capping agent) was added over 100 mL of $CdCl_2 \cdot H_2O$ (0.1 M), followed by dropping 50 mL of $Na_2S \cdot 9H_2O$ (0.1 M) until the reaction mixture

transformed into a bright orange color. The formed CdS particles were stirred for 16 h at 75 °C and then separated by centrifugation. The CdS particles were washed with double-distilled water and EtOH to remove the residual ions, then dried at 60 °C for 6 h.

Notably, the protein-containing mushroom extract could act as a capping agent during the fabrication of CdS, where it was proposed that it binds to the dissociated Cd^{2+} from $CdCl_2 \cdot 6H_2O$. When the Na_2S solution was dropped over the Cd/mushroom solution, it dissociates into S^{2-}, which directly binds to the mushroom's protein. Then, the nuclei of CdS grow following Ostwald ripening, resulting in CdS formation.[28]

2.3. Fabrication of PEI-modified BC

Firstly, BC was prepared from coffee waste as follows: collecting the coffee dregs and keeping them for drying naturally. The well-dried coffee dregs were pyrolyzed for 3 h at 500 °C under a controlled oxygen-limited environment. Secondly, 5.0 g of the BC powder was suspended in 300 mL of PEI/MeOH solution (10% w/v) at 35 °C under a slow stirring rate for a day. Then, aqueous glutaraldehyde solution (1% w/v) was mixed with the reaction suspension with continual stirring of almost 2 h for cross-linking. The black solid of PEI-BC was centrifugated, washed, and dried at 100 °C for 12 h.

2.4. Fabrication of CdS/PEI-BC/CTS

The CdS/PEI-BC/CTS composite was fabricated by the simple post-synthetic method. 50 mg of CTS was dissolved in 25 mL of double-distilled water (2% v/v acetic acid), then 100 mg of CdS and 50 mg of PEI-BC were added into the CTS solution. Next, the obtained solution of CdS/PEI-BC/CTS remained under sonication for 2 h. Then, the formed homogeneous CdS/PEI-BC/CTS composite was dried for 6 h at 70 °C in an oven. Notably, the CdS/PEI-BC/CTS composite was fabricated with other two ratios of CdS : PEI-BC : CTS, *i.e.*, 1 : 2 : 1 and 1 : 1 : 2.

2.5. Characterization tools

Fourier Transform Infrared (FTIR; Tensor II, Bruker), X-ray Diffraction (XRD; MAC Science M03XHF), Scanning Electron Microscopy (SEM; S4800, Hitachi), Zeta Potential (ZP; Malvern), ICP spectroscopy (ICP-OES; Agilent 5110), and X-ray Photoelectron Spectroscopy (XPS; Thermo-Fisher Sci.).

2.6. Batch experiments

The practical experiments to optimize the conditions of the Cr(VI) adsorption process onto the CdS/PEI-BC/CTS composite proceeded as follows: (i) examining the adsorption capacity of CdS/PEI-BC/CTS toward adsorbing Cr(VI) at different pH values; 3, 5, 7, 9, and 11 [adsorbent dose = 0.5 g L^{-1}, Cr(VI) concentration = 50 mg L^{-1}, and temperature = 20 °C]. (ii) Investigating the favorable adsorbent dose by varying the mass of CdS/PEI-BC/CTS between 0.005 and 0.015 g and recording its adsorption aptitude [pH = 3, Cr(VI) concentration = 50 mg L^{-1}, and temperature = 20 °C]. (iii) Studying the temperature influence on the Cr(VI) adsorption efficacy by elevating the temperature of the adsorption system from 20 to 50 °C [adsorbent dose = 0.5 g L^{-1}, Cr(VI) concentration = 50 mg L^{-1} and pH = 3]. (iv) Inspecting the adsorbability of CdS/PEI-BC/CTS in a wide concentration range of Cr(VI) between 50 and 300 mg L^{-1} [adsorbent dose = 0.5 g L^{-1}, pH = 3, and temperature = 20 °C]. (v) The impact of co-interfering anions has been evaluated by separately soaking chloride, sulfate, and nitrate in the concentration range of 10–30 mg L^{-1} for the adsorption of Cr(VI) by the CdS/PEI-BC/CTS system [adsorbent dose = 0.5 g L^{-1}, Cr(VI) concentration = 50 mg L^{-1}, pH = 3, and temperature = 20 °C]. The adsorption capacity (q_t) and removal percent (R%) of the adsorbed Cr(VI) species onto the surface of CdS/PEI-BC/CTS were determined by measuring the initial (C_o) and final (C_f) concentrations of Cr(VI) using a spectrophotometer and fill in with these concentrations in eqn (1) and (2), where V is the Cr(VI) volume (20 mL) and m is the CdS/PEI-BC/CTS mass (10 mg).

$$q_t = \frac{(C_o - C_f) \times V}{m} \quad (1)$$

$$R\% = \frac{C_o - C_f}{C_o} \times 100 \quad (2)$$

3. Results and discussion

3.1. Characterization of CdS/PEI-BC/CTS

3.1.1. Chemical composition. The FTIR spectra of CdS, BC, PEI-BC, CTS, and CdS/PEI-BC/CTS are given in Fig. 1A. The CTS spectrum revealed the distinctive peaks of N–H and O–H at 1558 and 3417 cm^{-1}, respectively. Moreover, the FTIR peaks of C–O, C–OH, and C–H manifested at 1015, 1401, and 2920 cm^{-1}.[29] The mushroom-derived CdS showed the distinctive peak of Cd–S at 621 cm^{-1}, and the peak at 1100 cm^{-1} is attributed to the sulfide compound.[30] The manifested peak at 1619 cm^{-1} is ascribed to the amide I-containing protein in mushrooms, and the peak belonging to the carboxyl group appeared at 1398 cm^{-1}.[28,31,32] The BC spectrum represented its distinguishing band at 797 and 1088 cm^{-1}, which are ascribed to C–H and C–O, respectively. In addition, the corresponding FTIR peaks to Si–O, O–C=O and C=O manifested at 458, 1486, and 1509 cm^{-1}.[33] The spectrum of PEI-BC revealed the distinctive peaks to C–N at 1223 cm^{-1}. The accompanying peaks to symmetric and asymmetric CH_2 of PEI manifested at 2900 and 2807 cm^{-1}, confirming the functionalization of BC with PEI.[34–36] The combination between PEI-BC, CTS, and CTS was proved by the FTIR spectrum of CdS/PEI-BC/CTS, which represented the characteristic bands to the neat components.

3.1.2. Crystalline phase. Fig. 2B revealed the crystallographic characteristics of CdS, BC, PEI-BC, CTS, and CdS/PEI-BC/CTS. The CTS pattern illustrated its corresponding peaks at 2-theta of 10° and 20°, accompanied by the planes of (240) and (273), respectively. The low peak intensity of CTS indicates its poor crystallinity, which is a common character not only in CTS but also in the whole polysaccharide polymers.[14] The CdS pattern illustrates its distinctive XRD peaks at 2-theta of 28.08°, 51.89°, 25.33°, 43.80°, 71.26°, 26.61°, 36.77°, and 47.90°, which are accompanied by the (101), (112), (100), (110), (211), (002),

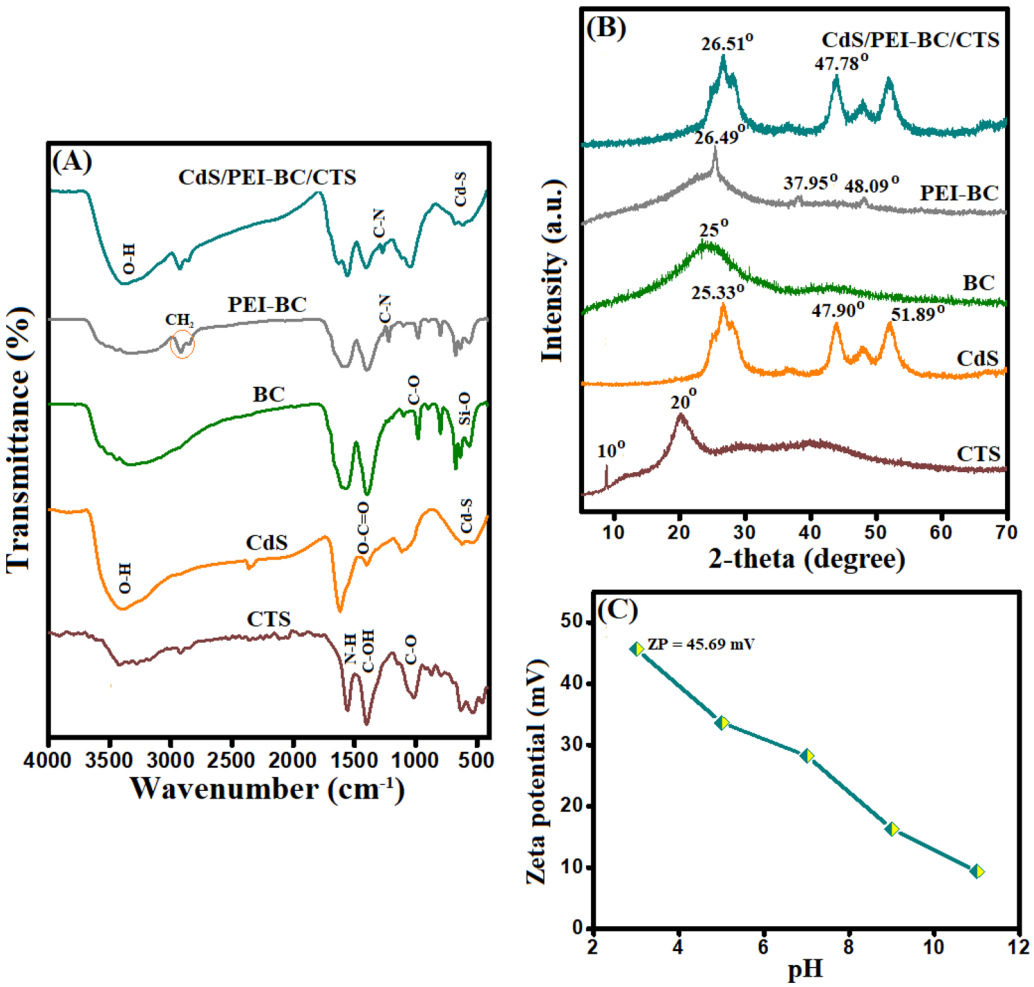

Fig. 1 (A) FTIR and (B) XRD of CTS, CdS, BC, PEI-BC, and CdS/PEI-BC/CTS. (C) Zeta potential of CdS/PEI-BC/CTS.

(102), and (103) planes, respectively.[37] The BC pattern showed its typical amorphous character since a wide broad peak manifested at 2-theta of 25°.[38] The crystallographic pattern of PEI-modified BC revealed the diffraction peaks of PEI at 2-theta of 26.49°, 37.95°, and 48.09°, evincing the cross-linkage of PEI with BC.[39] The low crystalline phases of CTS and PEI-BC prevent the appearance of their characteristic peaks in the CdS/PEI-BC/CTS pattern and decline the peak intensity of the corresponding peaks to CdS.

3.1.3. Surface charge. Actually, most adsorption systems are controlled mainly by electrostatic interactions between adsorbents and adsorbates. Therefore, measuring the surface charge of the adsorbent is a significant aspect of proving the occurrence possibility of electrostatic interactions. The CdS/PEI-BC/CTS composite carries positive charges, even in acidic or alkaline media, as elucidated from the zeta potential results in Fig. 1c. Furthermore, higher positive charges were detected on the CdS/PEI-BC/CTS composite (ZP = 45.69 mV) in a highly acidic medium. This observation inferred the suitability of the CdS/PEI-BC/CTS composite to adsorb anionic pollutants.

3.1.4. Surface morphology. Fig. 2A–E exhibits the morphology of CdS, BC, PEI-BC, CTS, and CdS/PEI-BC/CTS. The SEM image clarified the bipyramidal-like morphology of the green CdS with irregular size. The morphology of coffee waste-derived BC looks like rocky stacked layers, forming wide cavities. The PEI-BC image clarified distributed particles on the surface of BC and inside its cavities, which proved the successful cross-linage of PEI to BC. The CTS shape appeared as a rough sheet, clarifying the capability of CTS to be a supporter. The SEM image of the CdS/PEI-BC/CTS composite manifested the distribution of CdS and PEI-BC on the layers of CTS.

3.1.5. Elemental composition. The elemental composition of the CdS/PEI-BC/CTS composite is represented in Fig. 3A–F. The wide-spectrum illustrated the distinctive peaks of cadmium, oxygen, carbon, sulfur, and nitrogen at 406.11, 533.99, 287.14, 162.91, and 405.08 eV with atomic% of 4.3, 27.32, 62.62, 4.03, and 1.73%, respectively. The cadmium spectrum showed the corresponding peaks for Cd–S of $3d_{5/2}$ and $3d_{3/2}$ at 408.40 and 415.43 eV, in addition to the Cd–O peaks of $3d_{5/2}$ and $3d_{3/2}$ manifested at 405.31 and 412.09 eV, respectively.[40] The oxygen spectrum revealed the peaks of O–N, O–H, and O–C at 532.15, 533.23, and 535.83 eV, respectively.[41] The carbon spectrum depicted the carbon-based functional groups of C–C/C=C, C–N, C=O, and O=C–OH at 284.07, 285.88, 288.20, and 290.68 eV.[42,43] The spectrum of sulfur showed the relative peaks to S–Cd at 161.56 and 162.89 eV, while the peak of

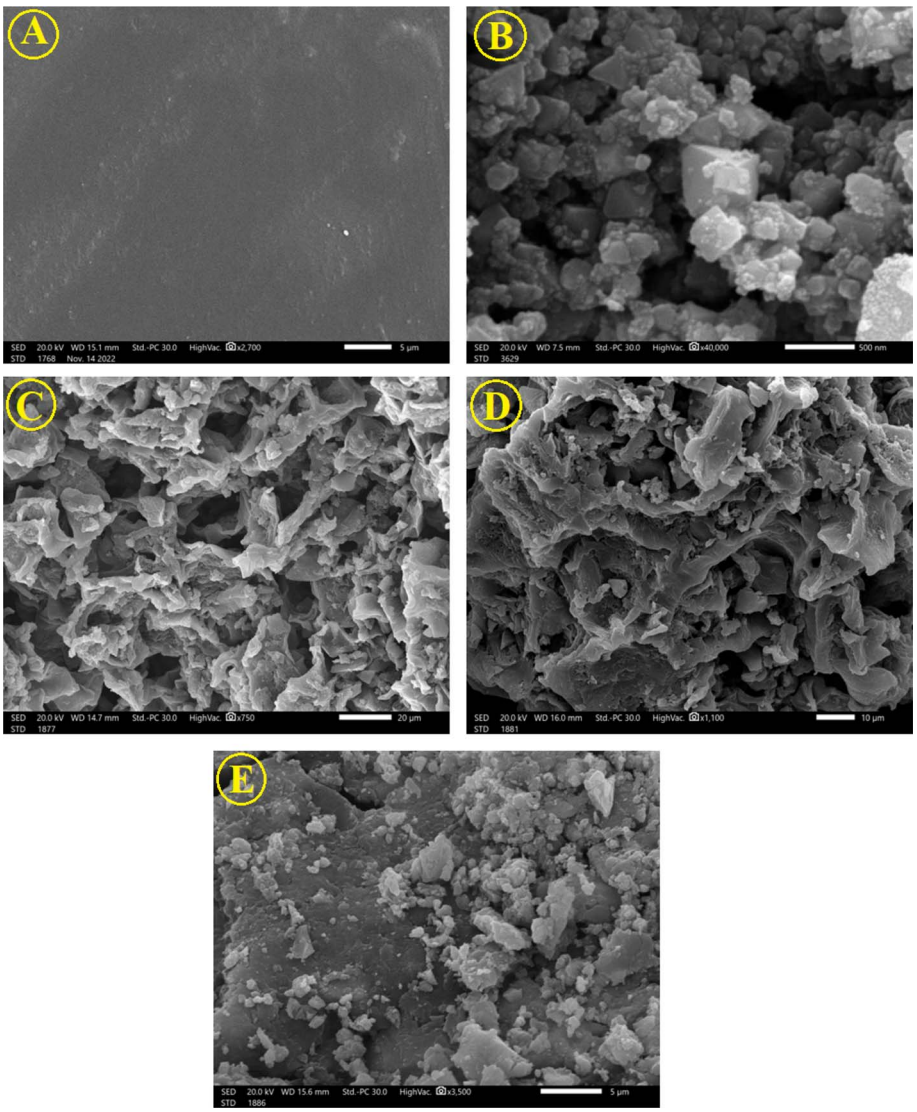

Fig. 2 SEM images of (A) CTS, (B) CdS, (C) BC, (D) PEI-BC, and (E) CdS/PEI-BC/CTS composite.

S–C appeared at 165.90 eV.[44] The characteristic peaks for N–H and NH_2 appeared in the nitrogen spectrum at 399.14 and 400.18 eV, respectively.[42]

3.2. Optimization of the Cr(VI) adsorption

3.2.1. Identifying the finest component ratio. The adsorption capabilities of the CdS/PEI-BC/CTS composites toward Cr(VI) were inspected to determine the best mass ratio between CdS, PEI-BC, and CTS, as represented in Fig. 4A. By comparing the adsorbability of the three composites towards Cr(VI), the optimal mass ratio between CdS : PEI-BC : CTS was 2 : 1 : 1 [pH = 3, adsorbent dose = 0.01 g, Cr(VI) concentration = 50 mg L^{-1}, and temperature = 20 °C] since R% and q_e were 97.89% and 98.09 mg g^{-1}, respectively. Furthermore, the removal aptitudes of Cr(VI) by CdS, BC, PEI-BC, and CTS were studied to confirm the significance of the synergistic effect between the authentic components in forming a composite with a higher adsorption performance. The R% of Cr(VI) onto CdS, BC, PEI-BC, and CTS were 74.39, 22.16, 43.13, and 53.16%, and the q_e values were 76.79, 29.47, 48.47, and 57.56 mg g^{-1}, respectively. This improvement in the removal efficacy of the Cr(VI) species by the CdS/PEI-BC/CTS composite, compared to the pristine materials, is due to the combination of the active adsorption sites of these components, which strengthens the interaction between the composite and Cr(VI) and increases the available mechanism pathways.

3.2.2. Identifying the optimal pH. It is well-known that Cr(VI) is a polyprotic species as it exists between pH 2 and 6 as $Cr_2O_7^{2-}$ and $HCrO_4^-$, while raising the pH of the medium over 6 changes the form of Cr(VI) to CrO_4^{2-}. Fig. 4B illustrates the effect of variation in the pH of the medium on the adsorption aptitude of Cr(VI) onto CdS/PEI-BC/CTS. A drastic decrease in the q and R% of Cr(VI) was observed from 97.86 mg g^{-1} and 97.83% to 24.66 mg g^{-1} and 23.37%, respectively, implying that pH 3 is the favorable medium to adsorb the Cr(VI) species onto CdS/PEI-BC/CTS. This result could be elucidated by protonating ample NH_2 groups on the CdS/PEI-BC/CTS backbone to NH_3 at a highly acidic medium, increasing the positive charges on the CdS/PEI-

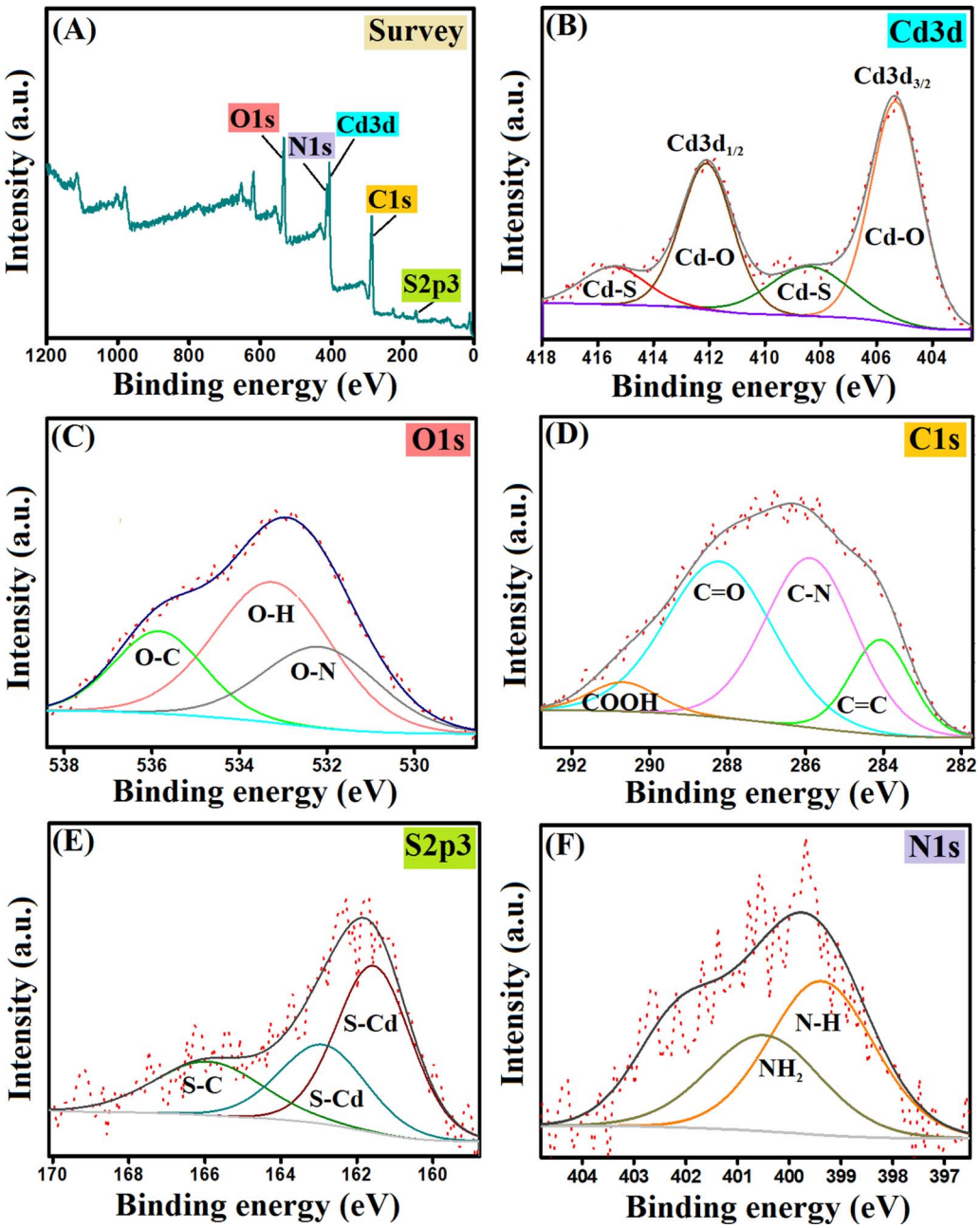

Fig. 3 The XPS spectra of the CdS/PEI-BC/CTS composite: (A) survey, (B) Cd 3d, (C) O 1s, (D) C 1s, (E) S 2p, and (F) N 1s.

BC/CTS composite.[45] This explanation was consistent with the zeta potential results that showed the high positive charges on the CdS/PEI-BC/CTS surface at pH = 3, where the zeta potential was 45.69 mV. Such an increase in the positive active groups on CdS/PEI-BC/CTS results in potent electrostatic interaction between the anionic Cr(VI) species and highly positive charges on the composite surface at pH 3.

3.2.3. Identifying the suitable adsorbent dosage. Fig. 4C depicts the experimental results of increasing the CdS/PEI-BC/CTS dosage on the adsorption% of Cr(VI). The adsorption capacity of Cr(VI) declined from 140.45 to 66.21 mg g^{-1} on increasing the CdS/PEI-BC/CTS dosage from 0.005 to 0.015 mg at the same Cr(VI) concentration, which is due to the increment in the un-occupied active binding sites. However, this elevation in the proportion of CdS/PEI-BC/CTS enhanced the removal% of Cr(VI) because of the superabundant binding sites to adsorb Cr(VI) at the higher adsorbent doses.[46,47] Hence, 0.01 mg could be selected as the suitable dose, taking into consideration the economic aspect.

3.2.4. Identifying the thermal nature. Actually, the temperature of the adsorbent system has a significant effect on constructing any adsorption process; thus, the adsorption% of Cr(VI) was examined at various temperatures between 20 and 50 °C, as represented in Fig. 4D. The improvement in the adsorbability of CdS/PEI-BC/CTS toward was Cr(VI) because the R% and q_e increased from 83.22% and 83.51 mg g^{-1} to 93.71%

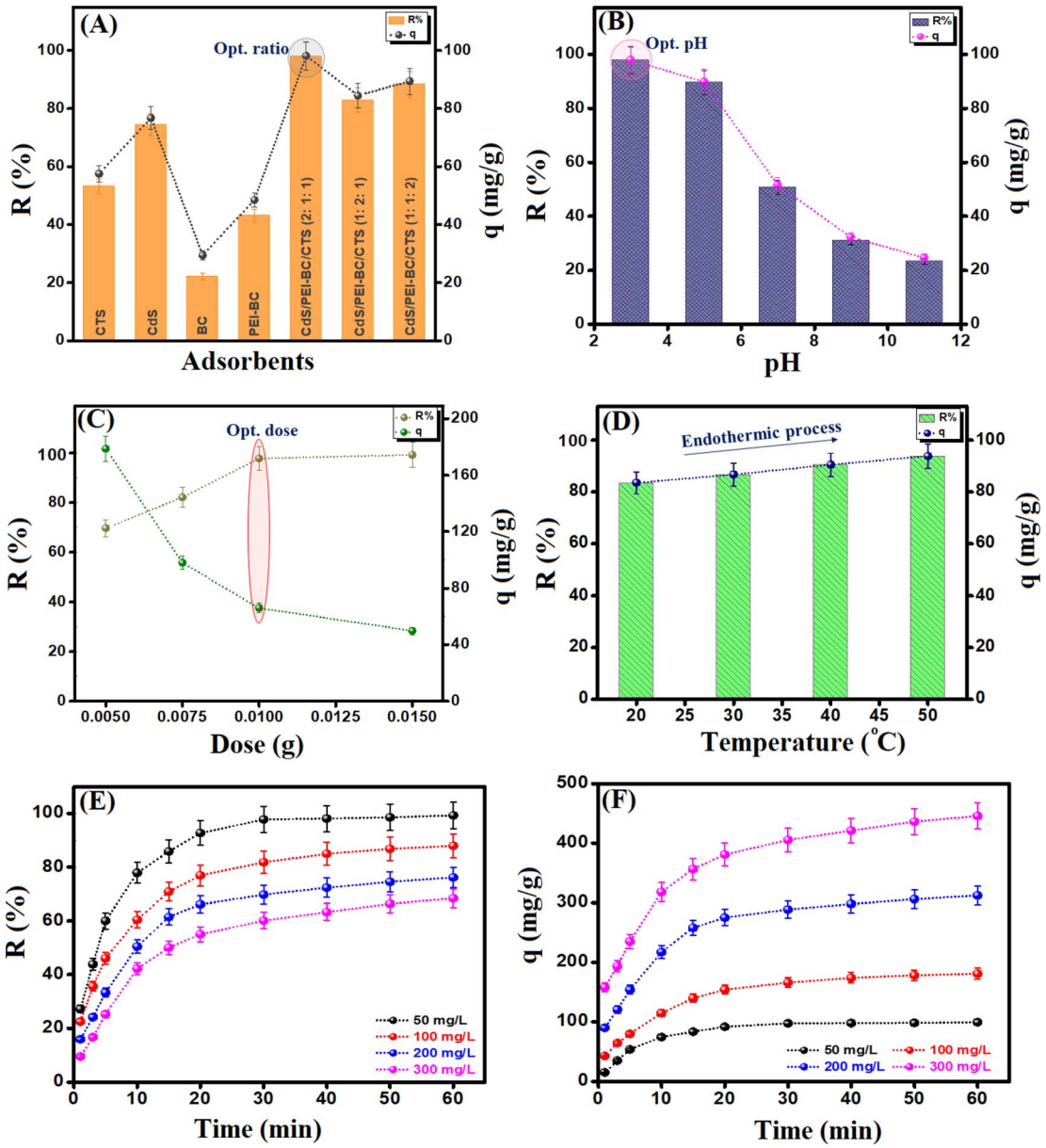

Fig. 4 Optimization of the Cr(VI) adsorption process: (A) comparison test, (B) identifying the optimal pH, (C) identifying the impact of the adsorbent dose, (D) identifying the thermodynamic behavior of the Cr(VI) adsorption process, and (E, F) identifying the influence of the initial Cr(VI) concentrations.

and 93.81 mg g^{-1}, respectively. This amelioration in the adsorption efficacy of Cr(VI) could result from the increase in the Brownian motion of the ions in the adsorption medium, which facilitates Cr(VI) to reach the CdS/PEI-BC/CTS surface.[48,49]

3.2.5. Identifying the concentration influence of Cr(VI). Fig. 4E and F represents the adsorption behavior of CdS/PEI-BC/CTS toward different concentrations of Cr(VI). The *R*% diminished from 99.28 to 68.39% with increasing Cr(VI) concentrations from 50 to 300 mg L^{-1} because of the inadequate active adsorption sites for the higher concentrations of Cr(VI). The *q* of Cr(VI) improved on raising the concentration from 99.16 to 445.65 mg L^{-1}, which could be allocated to the strengthening of the driving forces of the Cr(VI) species from the solution to the surface of CdS/PEI-BC/CTS.[50] Consequently, these strong driving forces could overcome the mass transfer resistance. The R% of Cr(VI) increased over time in all the studied concentrations and reached about 100% after one hour when the concentration of Cr(VI) was 50 mg L^{-1}. Furthermore, the adsorption aptitude of Cr(VI) by CdS/PEI-BC/CTS improved by increasing the adsorption time until the state of equilibrium was attained after half an hour.

3.3. The impact of co-interfering ions

In real applications, Cr(VI) is not the only anionic species in the adsorption system since there are several co-interfering species, as represented in Fig. 5A. Thus, some of these ions, such as chloride, nitrate, and sulfate, were separately added with

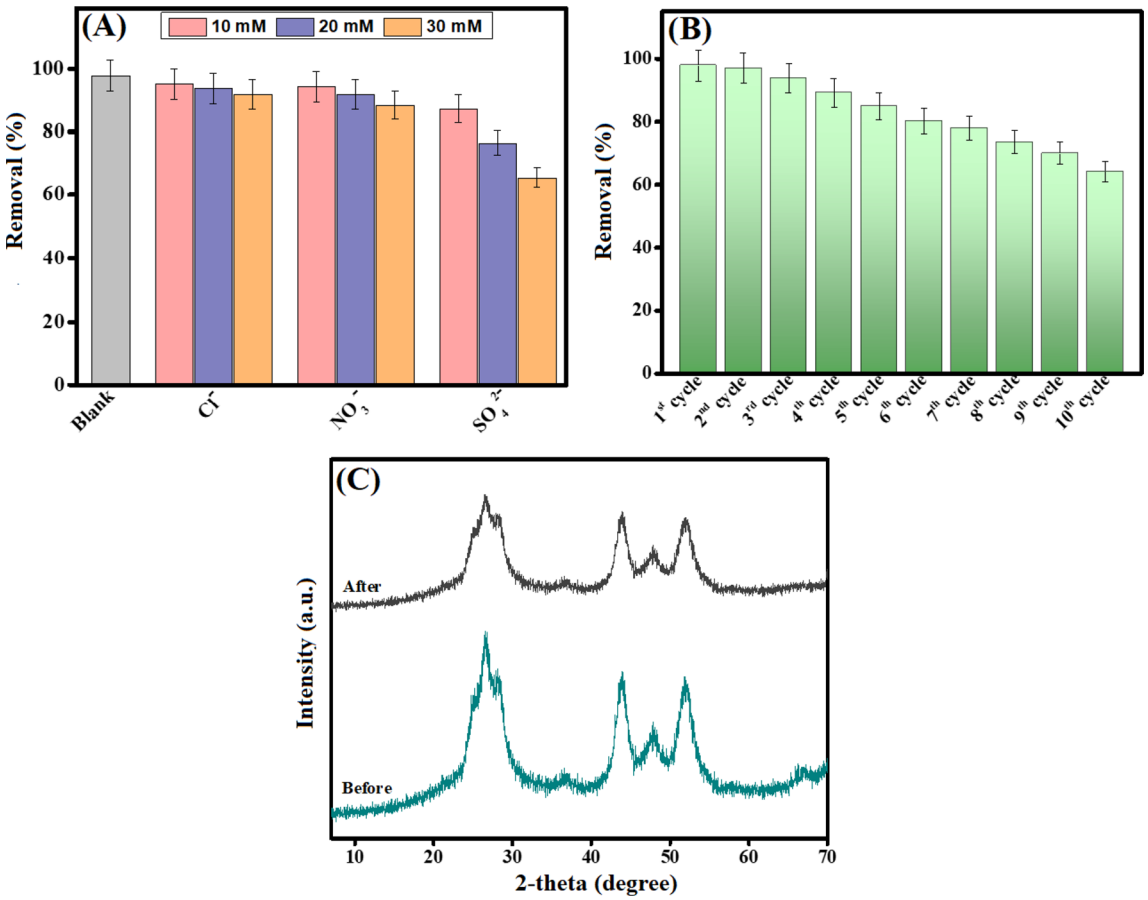

Fig. 5 (A) Effect of co-interfering ions, (B) recycling test of CdS/PEI-BC/CTS, and (C) XRD patterns of CdS/PEI-BC/CTS before and after the Cr(VI) adsorption process.

different concentrations to identify their impact on the removal aptitude of Cr(VI). The chloride species dwindled from 95.18 to 91.90% when elevating the chloride concentrations from 10 to 30 mg L^{-1}. In addition, the increase in the nitrate concentrations led to a decline in the removal% of Cr(VI) from 94.41 to 88.42%. This slightly less decrease in the removal efficacy of Cr(VI) could be explained by the weak-formed outer sphere complexation between these species and the CdS/PEI-BC/CTS composite. On the other hand, the sulfate species revealed a high computational effect on the Cr(VI) species, where the removal% of Cr(VI) declined from 87.30 to 65.59% with increasing concentrations.[5] This observation could be attributed to the ability of sulfate species to form inner and outer sphere complexes with the CdS/PEI-BC/CTS composite.

3.4. Recyclability study

After confirming the promising adsorption performance and high affinity of the CdS/PEI-BC/CTS composite, it was pivotal to assess its ability to be recycled and reused. The recyclability test was done ten times by collecting CdS/PEI-BC/CTS after each adsorption run and washing it using a mixture of methanol/NaCl as an eluent.[51] The results clarified that the recycling ability of CdS/PEI-BC/CTS was quite promising since its removal capacity towards Cr(VI) was still over 60% after recycling ten times, as demonstrated in Fig. 5B. This finding exhibited the applicability of the green-synthesized CdS/PEI-BC/CTS from eco-benign sources and its promising adsorbability, affinity, and recyclability toward the anionic Cr(VI) species.

3.5. Leaching test

To assure the eco-benign of the green-synthesized CdS/PEI-BC/CTS composite, the leaching concentrations of Cd were evaluated during the five adsorption cycles of Cr(VI) by ICP-OES. The leaching concentrations of the Cd species after the 1st, 2nd, 3rd, 4th, and 5th cycles were 0.2, 0.5, 0.8, 1.1, and 1.7 μg L^{-1}, respectively. Notably, the maximum contaminant level of the Cd ions allowed in drinking water by the EPA is 5.0 μg L^{-1}. These findings demonstrated that CdS/PEI-BC/CTS is an eco-friendly catalyst and does not become a secondary pollutant after the Cr(VI) adsorption process.

3.6. Chemical stability

The recycling study and leaching test confirmed the durability and non-toxicity of the CdS/PEI-BC/CTS composite. These findings could be explained by proving the chemical stability of CdS/PEI-BC/CTS. The XRD patterns of the neat and used CdS/PEI-BC/CTS composites were compared to demonstrate the chemical stability of the fabricated composite, as shown in Fig.

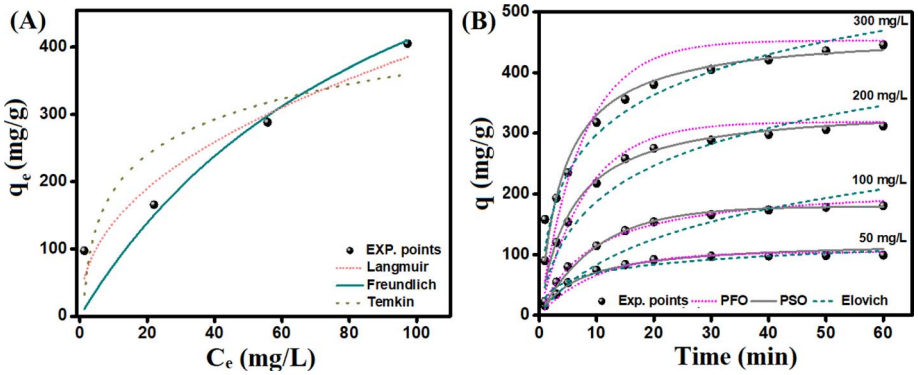

Fig. 6 (A) Isotherm study and (B) kinetic study for Cr(VI) adsorption onto the CdS/PEI-BC/CTS composite.

5C. Interestingly, the XRD patterns of the used CdS/PEI-BC/CTS composite elucidated the same diffraction peaks of the fresh composite with a slight decline in the peaks' intensity, implying the chemical stability of CdS/PEI-BC/CTS.

3.7. Mechanism study

3.7.1. Isotherms study. The nonlinear isotherms models, including Langmuir, Temkin, and Freundlich, were applied on the equilibrium data of Cr(VI) adsorption onto CdS/PEI-BC/CTS to identify the pathway of the Cr(VI) adsorption mechanism (Fig. 6A). Table S1† represents the nonlinear equations of the isotherm models. The evoked parameters from the isotherm plots denoted the fitness of the Freundlich model for Cr(VI) adsorption onto the surface of CdS/PEI-BC/CTS, in which the R^2 of the Freundlich model is the highest. In addition, the b value of the Temkin model was lower than 80 kJ mol^{-1}. Hence, it could be deduced from the Freundlich and Temkin models that adsorption of Cr(VI) onto CdS/PEI-BC/CTS was physical. The maximum capacity of CdS/PEI-BC/CTS to adsorb Cr(VI) was found to be 513.43 mg g^{-1}, based on the Langmuir findings. Besides, the n value elucidated the surface suitability of CdS/PEI-BC/CTS to adsorb the Cr(VI) species (Table 1).

Table 1 The parameters of the applied nonlinear isotherm models for Cr(VI) adsorption onto the CdS/PEI-BC/CTS composite

Isotherm model	Parameters	Value
Langmuir	q_{max} (mg g^{-1})	513.43
	K_L (L mg^{-1})	0.010
	R^2	0.858
Freundlich	n	2.24
	K_f	49.94
	R^2	0.941
Temkin	A (L g^{-1})	1.17
	b (kJ mol^{-1})	32.58
	R^2	0.752

3.7.2. Kinetics study. The kinetics study was done on the acquired data from the Cr(VI) adsorption process onto CdS/PEI-BC/CTS using nonlinear expressions of Elovich, Pseudo Second Order (PSO), and Pseudo First Order (PFO) to determine the adsorption pathway (Fig. 6B). The nonlinear kinetic equations are summarized in Table S2.† The PSO was found to be the most convenient kinetic model to clarify the adsorption pathway of Cr(VI) since its R^2 values for the inspected concentrations of Cr(VI) were the highest (Table 2). Hence, the adsorption of the

Table 2 The parameters of the applied nonlinear kinetic models for Cr(VI) adsorption onto the CdS/PEI-BC/CTS composite

Kinetic models and parameters	Concentration (mg L^{-1})			
	50	100	200	300
$q_{e,\ exp.}$ (mg g^{-1})	97.41	166.03	288.55	405.34
PFO				
$q_{e,\ cal.}$ (mg g^{-1})	144.21	159.64	308.68	352.90
k_1 (min^{-1})	0.100	0.095	0.125	0.135
R^2	0.951	0.979	0.921	0.833
PSO				
$q_{e,\ cal.}$ (mg g^{-1})	122.59	216.81	346.84	467.52
k_2 (g mg^{-1} min^{-1})	0.0011	0.0005	0.0004	0.0002
R^2	0.973	0.995	0.976	0.952
Elovich				
α (mg g^{-1} min^{-1})	13.69	58.97	60.71	194.96
β (g mg^{-1})	0.049	0.011	0.010	0.009
R^2	0.936	0.843	0.875	0.954

Cr(VI) species occurred by its chemical interactions with CdS/PEI-BC/CTS. Furthermore, the rate constant of PSO diminished with increasing Cr(VI) concentrations, implying the chemisorption of Cr(VI) onto the composite. Noteworthily, the computed adsorption rates of Cr(VI) from the Elovich model were found to be larger than the desorption rates, showing that the process is not irreversible.

3.7.3. Identifying the adsorbent/adsorbate interactions. As demonstrated from the kinetics study, the controlling interactions in the Cr(VI)/CdS/PEI-BC/CTS system are chemical, while the isotherm study implied the domination of the physical interactions. This result is not a conflict between the kinetics and isotherms studies but suggests two types of interactions during Cr(VI) adsorption onto CdS/PEI-BC/CTS. Consequently, the analysis tools, along with the experimental results, were inspected to determine the chemical and physical interactions between Cr(VI) and CdS/PEI-BC/CTS. The wide-spectrum of the Cr-adsorbed CdS/PEI-BC/CTS showed the existence of the Cr 2p peak at 579.45 eV, proving the occurrence of the adsorption process (Fig. 7A).

3.7.3.1. Physical interactions

3.7.3.1.1 Electrostatic interactions. It is well-known that electrostatic interaction is the most functional aspect of the adsorption system. For this purpose, while constructing our adsorption system, we engineered an adsorbent with cationic binding groups to adsorb the anionic Cr(VI) species. The highest

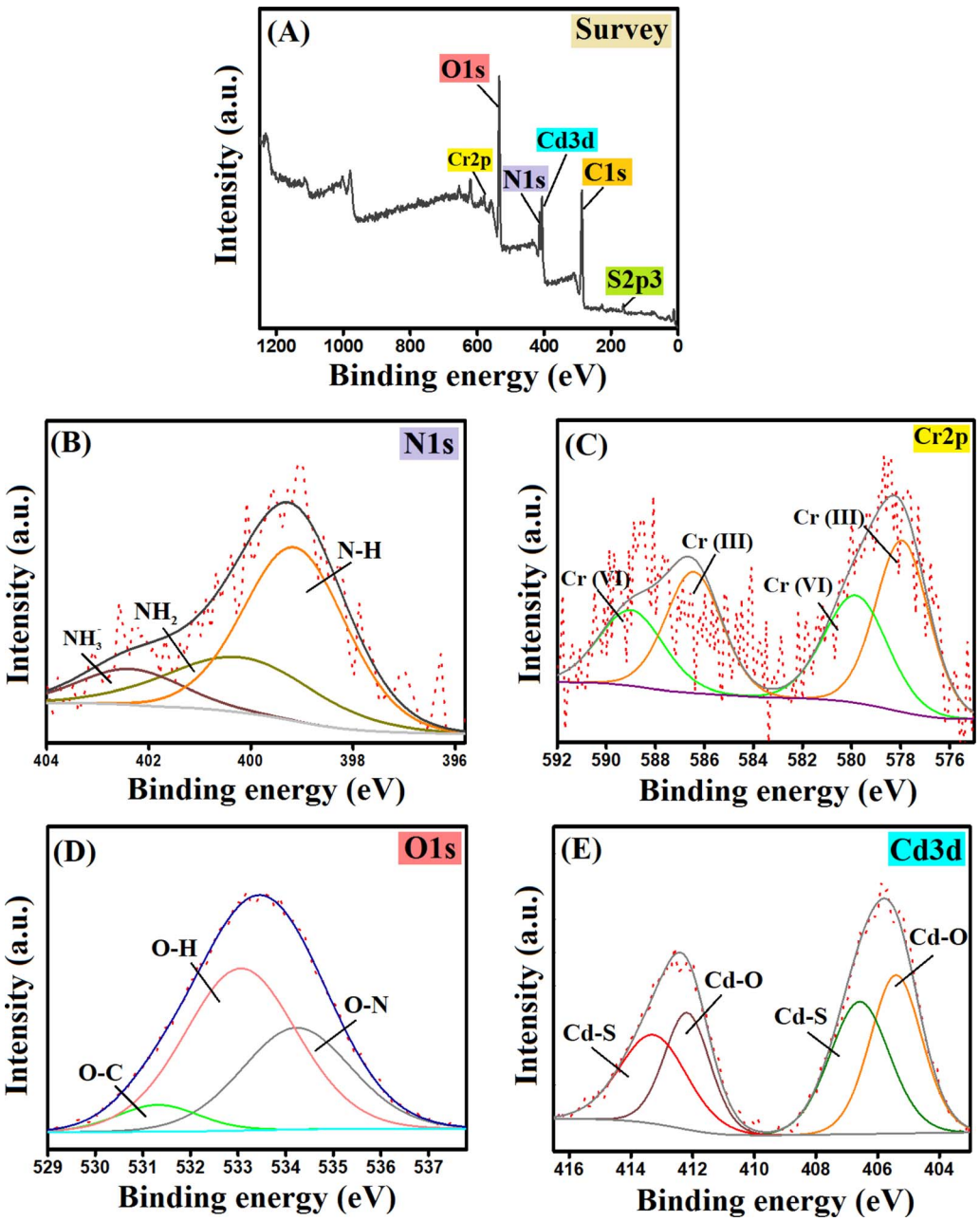

Fig. 7 The XPS spectra of the Cr(VI)-adsorbed CdS/PEI-BC/CTS composite: (A) survey, (B) N 1s, (C) Cr 2p, (D) O 1s, and (E) Cd 3d.

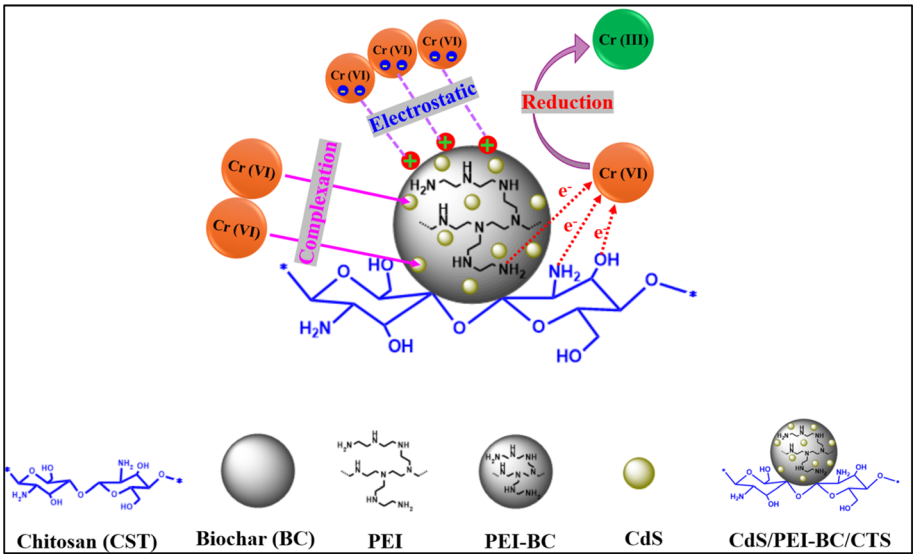

Fig. 8 Possible interactions between Cr(VI) and the CdS/PEI-BC/CTS composite.

ZP value of CdS/PEI-BC/CTS was 45.69 mV at pH 3, in addition to the experimental work that involved investigating the pH influence on the efficacy of Cr(VI) adsorption, implying that pH 3 is the most suitable. These clues confirmed the occurring potent electrostatic interaction between the CdS/PEI-BC/CTS composite and the Cr(VI) ions. Thanks to the ample amine groups of CTS and PEI-BC that are protonated in the acidic medium, high positive charges are present on the CdS/PEI-BC/CTS surface. This suggestion could be confirmed by the presence of the related peak for NH_3^+, as demonstrated in Fig. 7B.

3.7.3.2. Chemical interactions

3.7.3.2.1 Reduction mechanism. Many investigations regarding the adsorptive removal of Cr(VI) suggested the domination of the reduction mechanism that may be responsible for 50% of the total adsorbed Cr(VI) ions. The Cr 2p spectrum revealed the corresponding peaks for Cr(III) at 577.93 and 586.81 eV with atomic% of 33.19 and 11.26%, respectively. In addition, the peaks of Cr(VI) appeared at 579.82 and 589.45 eV, and their atomic% were 24.79 and 30.76%, respectively (Fig. 7C). Consequently, it was deduced that the atomic% of Cr(VI) and Cr(III) was 55.55 and 44.45%, respectively, reflecting the control of the reduction mechanism in the adsorption process of Cr(VI). The electron-rich groups like OH, NH_2, and COOH could donate electrons to reduce Cr(VI) to Cr(III). The red shift of OH (533.23–533.03 eV), COOH (290.68–289.40 eV), and NH_2 (400.71–400.18 eV), as elucidated in Fig. 7B and D, suggested the contribution of these functional groups to the adsorption of Cr(VI).

Table 3 Comparison study between the adsorbability of various adsorbents toward Cr(VI)

Adsorbent	q_{max} (mg g^{-1})	Eq. time (min)	Opt. pH	Adsorption mechanism	Ref.
ATP–CPBr@CA	302.11	120	2	Electrostatic interaction, ion-exchange, inner-/outer-complexation, reduction, pore-filling, and coordination bonds	52
ZnBDC/C-CTS	255	25	5	Electrostatic interaction and weak cation–π interaction	53
H_3PO_4-BC	245.70	720	2	Electrostatic interaction and reduction reaction	54
FeYBC	24.37	120	2.99–6.07	Complexation and reduction reaction	55
Fe_3O_4/ZIF-67@AmCTS	119.05	60	2	Electrostatic interaction, reduction reaction, and coordinate bonds	51
PANI@MCTS	186.60	15	2	Electrostatic interaction, complexation and reduction reaction	56
MPA-10	538.97	200	2	Electrostatic interaction, reduction reaction, and chelation interaction	57
GO-NH_2@CA-NH_2	410.21	60	2	Electrostatic interaction, reduction reaction, and coordinate–covalent bond	58
rGO/PEI-KOH	398.90	1440	2	Electrostatic interaction, reduction reaction, and chelation interaction	59
CTS-stabilized FeS	119.00	120	3	Electrostatic interaction and reduction reaction	25
CdS/PEI-BC/CTS	513.43	30	3	Electrostatic interaction, reduction reaction, and complexation	This study

3.7.3.2.2 Complexation. The complexation mechanism is one more effective pathway during the adsorption process of the Cr(VI) ions. Cd(II) could participate in the adsorption of both Cr(VI) and Cr(III) *via* the complexation mechanism by forming coordinate bonds between Cd(II) and the chromium species. The red shift of the XPS peaks in the Cd spectrum (Fig. 7E) reflected the contribution of the Cd species in the adsorptive removal of chromium ions. Also, the oxygenated groups of CdS/PEI-BC/CTS could chelate Cr(VI) and Cr(III) *via* the complexation mechanism.

All in all, the adsorption of Cr(VI) proceeded throughout four stages: (i) protonation of NH_2 to charge the CdS/PEI-BC/CTS surface with a positive charge. (ii) Electrostatic interactions that chelate the Cr(VI) species from their solution to the surface of CdS/PEI-BC/CTS. (iii) Reduction of the adsorbed Cr(VI) to the less toxic Cr(III). (iv) Coordinate bonds could be formed between Cr(VI) and Cr(III) and the CdS/PEI-BC/CTS composite, producing complexes. The possible interactions between Cr(VI) and CdS/PEI-BC/CTS are illustrated in Fig. 8.

3.8. Comparison study

A comparison study was performed between the adsorption performance of the CdS/PEI-BC/CTS composite toward Cr(VI) and the reported adsorbents in previous pioneering studies, taking into consideration the qmax, optimal pH, and equilibrium time, as depicted in Table 3.

4. Conclusion

The eco-friendly CdS/PEI-BC/CTS composite was fabricated by a simple green approach to adsorb Cr(VI) from wastewater. The best adsorption% was at pH = 3 because of the potent electrostatic interactions between Cr(VI) and the cationic active adsorption sites of the CdS/PEI-BC/CTS composite (ZP = 45.69 mV). The imitation of actual wastewater clarified the slight influence of chloride and nitrate on the Cr(VI) adsorption; however, the existence of sulfate manifested a significant impact on the adsorption% of Cr(VI). Interestingly, the CdS/PEI-BC/CTS composite revealed an excellent recycling ability during ten sequential adsorption runs. The kinetic and isotherm investigations denoted the combination of physical and chemical interactions for Cr(VI) adsorption. Furthermore, the characterization tools implied that the chemisorption of Cr(VI) proceeded by the complexation and reduction mechanisms, while the physisorption was controlled by the electrostatic interaction. Interestingly, the leaching test clarified the lower cadmium leaching concentration compared to the authorized concentration by EPA even after using the composite for five adsorption runs, denoting the eco-friendly merit of CdS/PEI-BC/CTS, which prevents the formation of a secondary pollutant after the Cr(VI) adsorption process.

In short, the CdS/PEI-BC/CTS composite has promising adsorbability, affinity, and reusability in the Cr(VI) adsorption process. However, the composite separation after the adsorption process needs a long time. Consequently, we recommend developing the separation of the CdS/PEI-BC/CTS composite by shaping it as a membrane or beads or incorporating a magnetic substance into the matrix of the composite. Furthermore, the shaping modification technique could also decline the leaching concentration of the Cd species after the adsorption process of Cr(VI).

Disclaimer/publisher's note

The statements, opinions and data contained in all publications are solely those of the individual author(s) and contributor(s).

Data availability

The data presented in this study are available on request from the corresponding authors.

Author contributions

Conceptualization, A. S. E., E. M. A., M. E. and N.·F. A.; methodology, A. S. E., E. M. A. and M. E.; software, A. S. E., E. M. A. and N.·F. A.; formal analysis, A. S. E., E. M. A. and N.·F. A.; investigation, A. S. E., E. M. A., M. E. and N.·F. A.; resources, A. S. E., E. M. A., M. E. and N.·F. A.; writing—original draft preparation, A. S. E., E. M. A. and N.·F. A.; writing—review and editing, M. E. and N.·F. A.; supervision, A. S. E. and E. M. A.; funding acquisition, A. S. E. and N.·F. A. All authors have read and agreed to the published version of the manuscript.

Conflicts of interest

The authors declare no conflicts of interest.

Acknowledgements

The Researchers would like to thank the Deanship of Graduate Studies and Scientific Research at Qassim University for financial support (QU-APC-2024-9/1).

References

1 K. E. Ukhurebor, *et al.*, Effect of hexavalent chromium on the environment and removal techniques: a review, *J. Environ. Manage.*, 2021, **280**, 111809.
2 A. Sharma, *et al.*, Chromium bioaccumulation and its impacts on plants: an overview, *Plants*, 2020, **9**(1), 100.
3 P. Madhusudan, C. Lee and J.-O. Kim, Synthesis of Al2O3@Fe2O3 core–shell nanorods and its potential for fast phosphate recovery and adsorption of chromium (VI) ions from contaminated wastewater, *Sep. Purif. Technol.*, 2023, **326**, 124691.
4 K. Kumaraguru, *et al.*, A systematic analysis of hexavalent chromium adsorption and elimination from aqueous environment using brown marine algae (Turbinaria ornata), *Biomass Convers. Biorefin.*, 2023, **13**(9), 8223–8238.
5 A. M. Omer, *et al.*, Construction of efficient Ni-FeLDH@MWCNT@ Cellulose acetate floatable microbeads for

Cr(VI) removal: performance and mechanism, *Carbohydr. Polym.*, 2023, **311**, 120771.
6 A. S. Eltaweil, *et al.*, Magnetic hierarchical flower-like Fe3O4@ ZIF-67/CuNiMn-LDH catalyst with enhanced redox cycle for Fenton-like degradation of Congo red: optimization and mechanism, *Environ. Sci. Pollut. Res.*, 2023, 1–17.
7 E. M. Abd El-Monaem, *et al.*, Enhanced Redox Cycle of Rod-Shaped MIL-88A/SnFe2O4@ MXene Sheets for Fenton-like Degradation of Congo Red; Optimization and Mechanism, *Nanomaterials*, 2023, **14**(1), 54.
8 Y. Liu, *et al.*, Ferrous disulfide and iron nitride sites on hydrochar to enhance synergistic adsorption and reduction of hexavalent chromium, *Bioresour. Technol.*, 2023, **388**, 129770.
9 C. Wu, *et al.*, Reduction and precipitation of chromium (VI) using a palladized membrane biofilm reactor, *Water Res.*, 2024, **249**, 120878.
10 S. M. El-Sheikh, *et al.*, Visible-light-driven 3D hierarchical Bi2S3/BiOBr hybrid structure for superior photocatalytic Cr(VI) reduction, *J. Alloys Compd.*, 2021, **857**, 157513.
11 R. Geioushy, *et al.*, One-pot fabrication of BiPO4/Bi2S3 hybrid structures for visible-light driven reduction of hazardous Cr(VI), *J. Hazard. Mater.*, 2020, **381**, 120955.
12 B. Liu, *et al.*, Removal of Chromium Species by Adsorption: Fundamental Principles, Newly Developed Adsorbents and Future Perspectives, *Molecules*, 2023, **28**(2), 639.
13 R. Garg, *et al.*, Rapid adsorptive removal of chromium from wastewater using walnut-derived biosorbents, *Sci. Rep.*, 2023, **13**(1), 6859.
14 E. M. Abd El-Monaem, A. M. Omer and A. S. Eltaweil, Durable and Low-Cost Chitosan Decorated Fe/MOF-5 Bimetallic MOF Composite Film for High Performance of the Congo Red Adsorption, *J. Polym. Environ.*, 2023, 1–16.
15 R. S. Riseh, M. G. Vazvani and J. F. Kennedy, The application of chitosan as a carrier for fertilizer: a review, *Int. J. Biol. Macromol.*, 2023, 126483.
16 W. Tang, *et al.*, Application of chitosan and its derivatives in medical materials, *Int. J. Biol. Macromol.*, 2023, 124398.
17 A. N. Doyo, R. Kumar and M. Barakat, Recent advances in cellulose, chitosan, and alginate based biopolymeric composites for adsorption of heavy metals from wastewater, *J. Taiwan Inst. Chem. Eng.*, 2023, **151**, 105095.
18 K. Wang, *et al.*, Modified magnetic chitosan materials for heavy metal adsorption: a review, *RSC Adv.*, 2023, **13**(10), 6713–6736.
19 H. Majiya, F. Clegg and C. Sammon, Bentonite-Chitosan composites or beads for lead (Pb) adsorption: design, preparation, and characterisation, *Appl. Clay Sci.*, 2023, **246**, 107180.
20 H. Alyasi, H. Mackey and G. McKay, Adsorption of Methyl Orange from Water Using Chitosan Bead-like Materials, *Molecules*, 2023, **28**(18), 6561.
21 C. V. Gopi, *et al.*, A strategy to improve the energy conversion efficiency and stability of quantum dot-sensitized solar cells using manganese-doped cadmium sulfide quantum dots, *Dalton Trans.*, 2015, **44**(2), 630–638.
22 M. D. Rao and G. Pennathur, Green synthesis and characterization of cadmium sulphide nanoparticles from Chlamydomonas reinhardtii and their application as photocatalysts, *Mater. Res. Bull.*, 2017, **85**, 64–73.
23 S. M. Shaheen, *et al.*, Wood-based biochar for the removal of potentially toxic elements in water and wastewater: a critical review, *Int. Mater. Rev.*, 2019, **64**(4), 216–247.
24 R. Deng, *et al.*, Biochar-mediated Fenton-like reaction for the degradation of sulfamethazine: role of environmentally persistent free radicals, *Chemosphere*, 2020, **255**, 126975.
25 H. Zhang, *et al.*, Chitosan-stabilized FeS magnetic composites for chromium removal: characterization, performance, mechanism, and stability, *Carbohydr. Polym.*, 2019, **214**, 276–285.
26 X. Liu, Y. Zhang and Y. Liu, Green method to synthesize magnetic zeolite/chitosan composites and adsorption of hexavalent chromium from aqueous solutions, *Int. J. Biol. Macromol.*, 2022, **194**, 746–754.
27 A. S. Eltaweil, *et al.*, Synthesis of a new magnetic Sulfacetamide-Ethylacetoacetate hydrazone-chitosan Schiff-base for Cr(VI) removal, *Int. J. Biol. Macromol.*, 2022, **222**, 1465–1475.
28 S. Tudu, *et al.*, CdS nanoparticles (< 5 nm): green synthesized using Termitomyces heimii mushroom–structural, optical and morphological studies, *Appl. Phys. A*, 2021, **127**, 1–9.
29 S. Yasmeen, *et al.*, Chromium (VI) ions removal from tannery effluent using chitosan-microcrystalline cellulose composite as adsorbent, *Int. Res. J. Pure Appl. Chem.*, 2016, **10**(4), 1–14.
30 S. R. K. Pandian, *et al.*, Biologically synthesized fluorescent CdS NPs encapsulated by PHB, *Enzyme Microb. Technol.*, 2011, **48**(4–5), 319–325.
31 H. S. Mahdi, *et al.*, Microstructural and optical properties of sol gel synthesized CdS nano particles using CTAB as a surfactant, in *AIP Conference Proceedings*, AIP Publishing, 2017.
32 S. Kumar and J. Sharma, Stable phase CdS nanoparticles for optoelectronics: a study on surface morphology, structural and optical characterization, *Mater. Sci.-Pol.*, 2016, **34**(2), 368–373.
33 E. Behazin, *et al.*, Mechanical, chemical, and physical properties of wood and perennial grass biochars for possible composite application, *BioResources*, 2016, **11**(1), 1334–1348.
34 J. Wang, *et al.*, Polyethyleneimine-functionalized mesoporous carbon nanosheets as metal-free catalysts for the selective oxidation of H2S at room temperature, *Appl. Catal., B*, 2021, **283**, 119650.
35 G. Herlem, T. Gharbi and N. B. Sedrine, Analyzing ab initio infrared spectra and electronic properties of polyethylenimine water complexes in the solid state, *J. Mol. Struct.: THEOCHEM*, 2010, **945**(1–3), 27–32.
36 H. Yankovych, *et al.*, New perception of Zn (II) and Mn (II) removal mechanism on sustainable sunflower biochar from alkaline batteries contaminated water, *J. Environ. Manage.*, 2021, **292**, 112757.

37 B. S. Rao, *et al.*, Preparation and characterization of CdS nanoparticles by chemical co-precipitation technique, *Chalcogenide Lett.*, 2011, **8**(3), 177–185.
38 M. Burachevskaya, *et al.*, Fabrication of biochar derived from different types of feedstocks as an efficient adsorbent for soil heavy metal removal, *Sci. Rep.*, 2023, **13**(1), 2020.
39 A. Sumisha, *et al.*, Functionalized titanate nanotube–polyetherimide nanocomposite membrane for improved salt rejection under low pressure nanofiltration, *RSC Adv.*, 2015, **5**(49), 39464–39473.
40 I. Mehmood, *et al.*, Investigation of silver doped CdS co-sensitized TiO2/CISe/Ag–CdS heterostructure for improved optoelectronic properties, *Opt. Mater.*, 2021, **111**, 110645.
41 J. Gomez-Bolivar, *et al.*, Synthesis of Pd/Ru bimetallic nanoparticles by Escherichia coli and potential as a catalyst for upgrading 5-hydroxymethyl furfural into liquid fuel precursors, *Front. Microbiol.*, 2019, **10**, 1276.
42 G. Simões dos Reis, *et al.*, Facile synthesis of sustainable activated biochars with different pore structures as efficient additive-carbon-free anodes for lithium-and sodium-ion batteries, *ACS Omega*, 2022, **7**(46), 42570–42581.
43 X. Cui, *et al.*, Application of a Novel Bifunctionalized Magnetic Biochar to Remove Cr(VI) from Wastewater: Performance and Mechanism, *Separations*, 2023, **10**(6), 358.
44 Y. Gu, *et al.*, Preparation and photoelectric properties of cadmium sulfide quantum dots, *Chin. Phys. B*, 2019, **28**(4), 047803.
45 V. Marjanović, *et al.*, Adsorption of chromium (VI) from aqueous solutions onto amine-functionalized natural and acid-activated sepiolites, *Appl. Clay Sci.*, 2013, **80**, 202–210.
46 F. Liu, *et al.*, Effective adsorption and immobilization of Cr(VI) and U (VI) from aqueous solution by magnetic amine-functionalized SBA-15, *Sep. Purif. Technol.*, 2022, **282**, 120042.
47 S. Nasanjargal, *et al.*, The removal of chromium (VI) from aqueous solution by amine-functionalized zeolite: Kinetics, thermodynamics, and equilibrium Study, *J. Environ. Prot.*, 2021, **12**(9), 654–675.
48 A. Nishino, *et al.*, Kinetic, isotherm, and equilibrium investigation of Cr(VI) Ion adsorption on amine-functionalized porous silica beads, *Polymers*, 2022, **14**(10), 2104.
49 K. Yamada, *et al.*, Hexavalent Cr ion adsorption and desorption behaviour of expanded poly (tetrafluoro) ethylene films grafted with 2-(dimethylamino) ethyl methacrylate, *Environ. Technol.*, 2021, **42**(12), 1885–1898.
50 A. M. Omer, *et al.*, Graphene oxide@ Fe3O4-decorated iota-carrageenan composite for ultra-fast and highly efficient adsorption of lead (II) from water, *Int. J. Biol. Macromol.*, 2023, **253**, 127437.
51 A. M. Omer, *et al.*, Facile fabrication of novel magnetic ZIF-67 MOF@ aminated chitosan composite beads for the adsorptive removal of Cr(VI) from aqueous solutions, *Carbohydr. Polym.*, 2021, **265**, 118084.
52 E. M. Abd El-Monaem, *et al.*, Construction of attapulgite decorated cetylpyridinium bromide/cellulose acetate composite beads for removal of Cr(VI) ions with emphasis on mechanistic insights, *Sci. Rep.*, 2024, **14**(1), 12164.
53 C. Niu, *et al.*, Preparation of a novel citric acid-crosslinked Zn-MOF/chitosan composite and application in adsorption of chromium (VI) and methyl orange from aqueous solution, *Carbohydr. Polym.*, 2021, **258**, 117644.
54 H. Zeng, *et al.*, Efficient adsorption of Cr(VI) from aqueous environments by phosphoric acid activated eucalyptus biochar, *J. Cleaner Prod.*, 2021, **286**, 124964.
55 F.-X. Dong, *et al.*, Simultaneous adsorption of Cr(VI) and phenol by biochar-based iron oxide composites in water: performance, kinetics and mechanism, *J. Hazard. Mater.*, 2021, **416**, 125930.
56 C. Lei, *et al.*, Polyaniline@ magnetic chitosan nanomaterials for highly efficient simultaneous adsorption and in-situ chemical reduction of hexavalent chromium: removal efficacy and mechanisms, *Sci. Total Environ.*, 2020, **733**, 139316.
57 Y. Feng, *et al.*, Fabrication of MXene/PEI functionalized sodium alginate aerogel and its excellent adsorption behavior for Cr(VI) and Congo Red from aqueous solution, *J. Hazard. Mater.*, 2021, **416**, 125777.
58 A. M. Omer, E. M. Abd El-Monaem and A. S. Eltaweil, Novel reusable amine-functionalized cellulose acetate beads impregnated aminated graphene oxide for adsorptive removal of hexavalent chromium ions, *Int. J. Biol. Macromol.*, 2022, **208**, 925–934.
59 Y. Tadjenant, *et al.*, Graphene oxide chemically reduced and functionalized with KOH-PEI for efficient Cr(VI) adsorption and reduction in acidic medium, *Chemosphere*, 2020, **258**, 127316.